Distribution of IR-UWB Signals with PAM modulation in FTTH networks

Tiago Valente

Instituto de Telecomunicações, Department of Electrical and Computer Engineering, Instituto Superior Técnico

Av. Rovisco Pais 1, 1049-001 Lisboa, Portugal

***Abstract*—Fiber-to-the-home (FTTH) networks have been proposed as a means to extend the application of ultra-wideband (UWB) signals in future wireless personal area networks (WPAN) to the delivery of high-definition content.**

In this paper, we analyze the feasibility of the distribution of impulse radio UWB (IR-UWB) signals with pulse amplitude modulation (PAM) in long reach FTTH networks. The simulation results obtained show that there is a severe performance degradation of the transmitted signals in this type of system, mainly due to the effect of the group velocity dispersion.

***Index Terms*—Optical communications, Fiber-to-the-home (FTTH) access networks, Impulse-radio ultra-wideband (IR-UWB), distortion.**

I. Introduction

Ultra-wideband (UWB) signals, approved by the Federal Communications Commission (FCC) for unlicensed use for a spectrum range from 3.1 GHz to 10.6 GHz [1], are recently emerging as a solution for the future wireless personal area networks (WPAN), due to their potential for high data rates, tolerance to multipath fading and low probability of interception at low cost and low power consumption [2] [3]. In order to extend its application to the delivery of high-definition (HD) contents, such as HD audio and video, in the access networks, the distribution of UWB signals over optical fiber has been considered an enabling technology [5], particularly within the context of the fiber-to-the-home (FTTH) access networks [6] [7]. The FTTH access networks are considered a suitable means for the distribution of UWB signals since they provide enough bandwidth for the transport of several UWB streams, do not require the transmodulation of the original UWB signals neither any frequency up-conversion [6] being, therefore, transparent to specific UWB implementations.

Currently, two major flavors are used for UWB communications: one is based on orthogonal frequency division multiplexing (OFDM), and the other one is based on the transmission and reception of very short duration pulses, named impulse radio UWB (IR-UWB) pulses. While the first technology (OFDM) is currently being adopted by the industry as the standard for most UWB communication systems in WPANs, the IR-UWB alternative presents some advantages: it does not require a carrier modulation scheme, uses simpler modulation schemes, such as Pulse Amplitude Modulation (PAM) or Pulse Position Modulation (PPM), exhibits a very short duty-cycle which minimizes the potential for interference with other radio signal, and benefits from a coding gain achieved through the use of time-hopping or direct-sequence spreading [2].

In this paper, we investigate the distribution of IR-UWB signals with PAM modulation and direct-sequence spreading in FTTH networks. In particular, we study the case of the Passive Optical Network (PON) solution for the FTTH access network, as it is considered the most promising optical access network architecture, in terms of cost-effectiveness, due to the infrastructure cost sharing between the customers and the reduction of the number of active components in the path between the central office and the customer [8].

The paper is structured as follows: in Section 2, we present the IR-UWB communication system as well as the signals used in this system, and analyze their time and spectral characteristics, namely in what concerns the compliance with the FCC standard that regulates UWB signals. In Section 3, we present the FTTH network used to distribute the considered IR-UWB signals, which is based on a PON architecture, and describe each of its components. We also describe the equivalent block diagram of the system to evaluate its performance. In Section 4, we present the methods used to assess the system performance, namely the time distortion factor, the spectral distortion factor and the channel error probability. In Section 5, we present the most important results of the investigation, obtained from MATLAB® simulations, and discuss the observed results. Finally, in Section 6, we draw the major conclusions of this work.

II. IR-UWB signals and IR-UWB communication system

The IR-UWB signals belong to the broader family of UWB signals. In 2002, the FCC issued UWB rulings that provided the first radiation limitations for UWB transmission and permitted the operation of UWB devices on an unlicensed basis [1]. According to such rulings, UWB signals are defined by having a fractional bandwidth greater than 0.2, or a signal

bandwidth greater than 500 MHz. The fractional bandwidth is defined as B / f_c, where $B = f_H - f_L$ represents the –10 dB bandwidth of the signal, $f_c = (f_H + f_L) / 2$ is the center frequency of the corresponding spectrum, and f_H and f_L denote the upper and lower frequency, respectively, measured at –10 dB below the peak emission point. Additionally, FCC has mandated that the UWB radio transmission can legally operate in the 3.1 to 10.6 GHz range, as long as the power spectral density (PSD) of the radiated signals comply with a defined spectral mask. As the FCC standard does not define a temporal waveform for the UWB signals, different approaches have been proposed (OFDM and IR-UWB). In this work, we focus on the IR-UWB case. In this case, the transmitted signals are composed by a sequence of very short pulses (with widths of the order of hundreds of picoseconds) without the need of carrier modulation. These short pulses are called base pulses and the data is modulated on them using either pulse amplitude modulation (PAM) or pulse position modulation (PPM). In order to support multiple users and signal encryption, time-hopping or direct-sequence (DS) spreading techniques may be used [2]. In this study, we consider only the PAM case with DS coding.

Considering the FCC standard, special care should be taken in selecting the waveforms to be used as base pulses, since these will significantly influence the spectrum of the radiated signal. Historically, Gaussian pulses and their time derivatives have been selected for the base pulses, namely the first derivative of the Gaussian pulse, which is generally known as monocycle. However, it has been shown [9] that the transmission of the pure Gaussian monocycle would not comply with the FCC requirements, being necessary to use higher-order derivatives of the Gaussian pulse, combinations of the derivatives of the Gaussian pulse or to filter the pulse to fit within the allowed bandwidth.

Since one of the requirements supporting the implementation of UWB wireless networks is to reduce the complexity needed for the equipments involved, our approach in this work is to use only pure Gaussian pulse or its derivatives as base pulses. As so, we have investigated the compliance of such pulses with the FCC spectral requirements. Considering the generic Gaussian pulse, whose waveform is given by [4]:

$$w(t) = -\sqrt{2} / \alpha \cdot \exp\left[-2 \cdot \pi \cdot \left(t / \alpha\right)^2\right], \qquad (1)$$

where α is the shape factor, it is known that, generally, if the pulse is transmitted by an antenna, the output of the transmitter antenna can be modeled by the first derivative of $w(t)$ [9]. The upper and lower frequencies of the radiated pulse, f_H and f_L, can then be determined as a function of the shape factor, α, the bit repetition period, T_{rep}, and number of bit repetitions, N_s. We have confirmed that the compliance with the spectral requirements of the FCC standard is only possible when the base pulses consist of Gaussian derivatives of the 3rd order or higher – the results for upper and lower frequencies of the radiated signal generated using as base pulse the 3rd order derivative of the Gaussian pulse are depicted in Fig. 1.

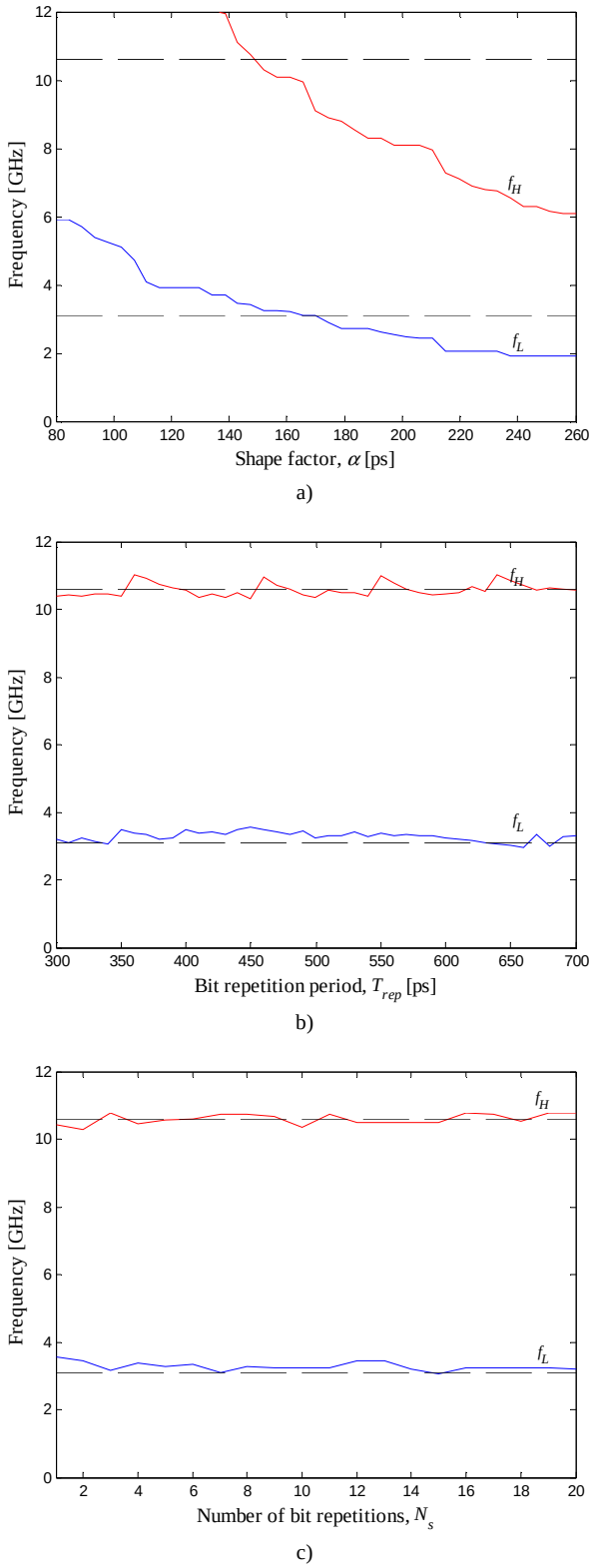

Fig. 1 Upper and lower frequencies for the radiated IR-UWB signal using the 3rd order Gaussian pulse derivative as base pulse as a function of a) the shape factor, considering $N_s = 10$ and $T_{rep} = 500$ ps, b) the bit repetition period, considering $N_s = 10$ and $\alpha = 150$ ps, and c) the number of bit repetitions, considering $\alpha = 150$ ps and $T_{rep} = 500$ ps.

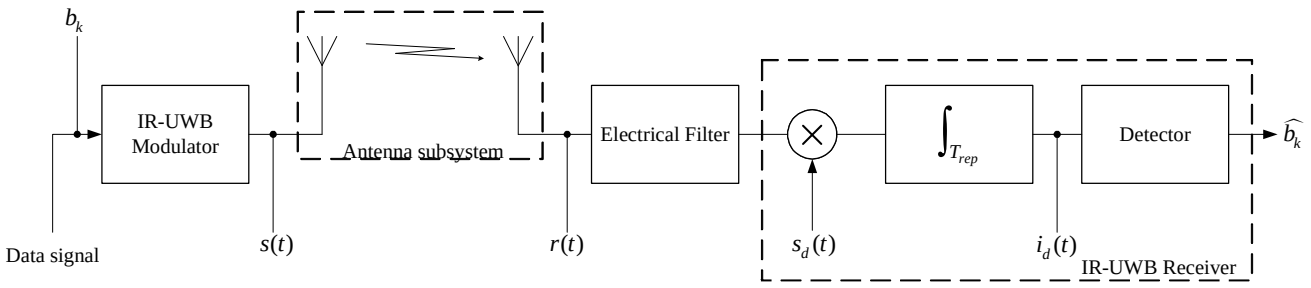

Fig. 2 Block diagram of an IR-UWB communication system

As can be observed in Fig. 1, the variations of the shape factor, α, have a strong influence on the location of the upper and lower frequency bounds of the signal spectrum. Changes in the other analyzed parameters, T_{rep} and N_s, have only a small influence on these locations.

Another important fact observed from the tests performed is that the range of values of the shape factor, for which the upper and lower bounds of the signal spectrum are located within the acceptable values, is enlarged with the increasing order of the Gaussian pulse derivative used for the base pulse.

The block diagram of the IR-UWB system as described above is depicted in Fig. 2. In Fig. 2, the IR-UWB modulator is responsible for the generation of the defined IR-UWB signal, *s(t)*, according to the bit sequence, b_k., to be transmitted The generated signal is then delivered to the antenna subsystem for the signal transmission through the air to the receiver. At the receiver front-end, the received signal, *r(t)*, is passed through an electrical filter, responsible for reducing the noise power added to the signal due to the thermal noise generated by the antennas. Finally, the signal is processed by the IR-UWB receiver, which realizes the correlation of the incoming signal with a signal $s_d(t)$, which is usually the base pulse and, depending on the result, produces an estimate of the transmitted bit.

III. Long Reach FTTH Network for the Distribution of IR-UWB Signals

The proposals for next generation FTTH networks are currently based on the PON architecture. Additionally, they make use of dense-wavelength division multiplexing (DWDM) technology in order to increase the utilization rate of the installed fiber in the metropolitan area and employ optical amplification to extend the transmission reach without the need for expensive optical-electrical-optical conversions in intermediate locations [10] [11] [12]. This approach is depicted in Fig. 3.

In the central node of the network, the signals are generated, wavelength-multiplexed and transmitted through single-mode fiber (SMF) to the local exchange. At the local exchange, an erbium-doped fiber amplifier (EDFA) increases the optical power of the received DWDM signal, in order to compensate for the power losses occurred during the transmission through the optical fiber as well as the ones due to component losses, such as connectors, splices and the optical splitters that will follow. The DWDM signal at the EDFA output is demultiplexed, and so each wavelength is separated and transmitted through different optical fibers. Each of these wavelengths will then be handled to an optical splitter, which will deliver the transmitted signal to a number of customers. The distance between the central node of the network and the

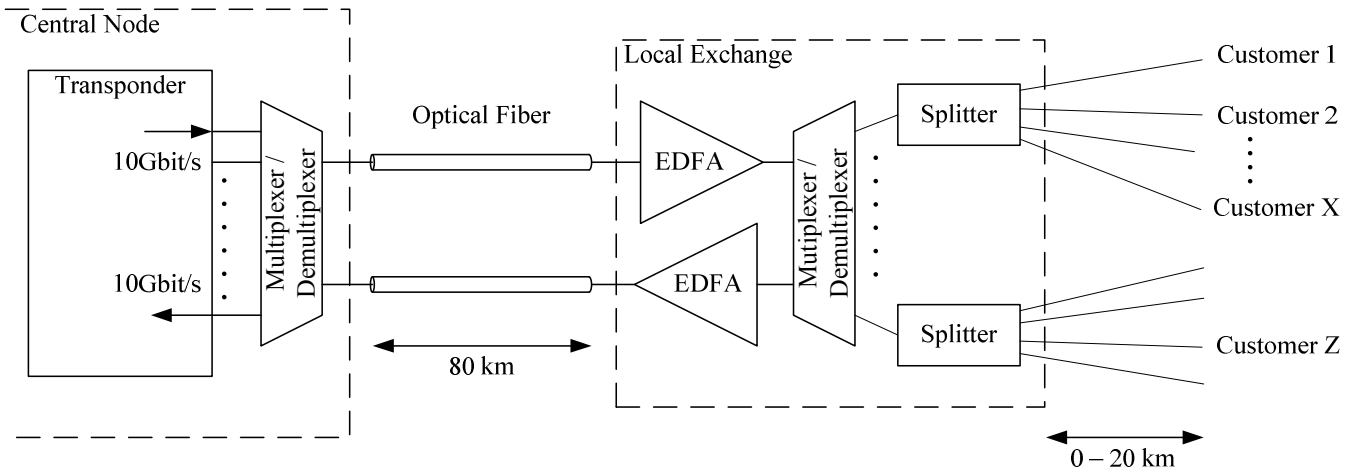

Fig. 3 Simplified scheme of an FTTH network employing DWDM and optical amplification

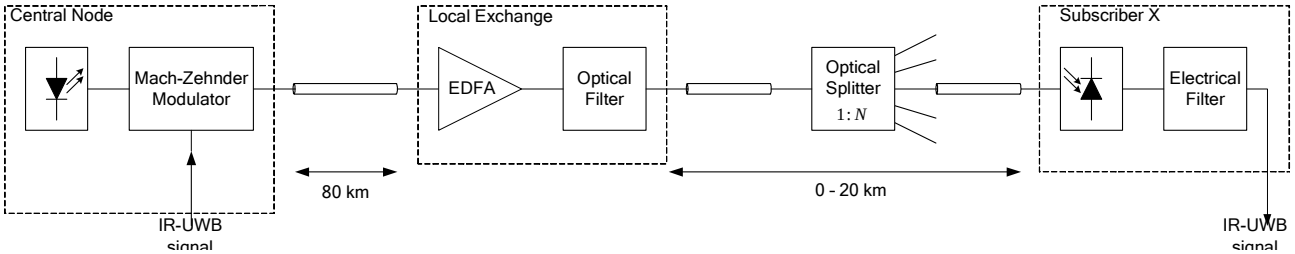

Fig. 4 Equivalent system model of the FTTH network with respect to the transmitted IR-UWB signal

local exchange is about 80 km and the distance from the local exchange to the customer premises is between 0 and 20 km.

Considering now the application scenario of this work, the IR-UWB communication system described in Section II shall be integrated into the long reach FTTH network described above. Since the IR-UWB signal is transmitted from the central node using just one of the many DWDM channels transmitted from the central node to the local exchange, we isolate the path of one channel through the FTTH network, and draw the corresponding equivalent system from the point of view of this path (which will be used for the transmission of the IR-UWB signal) in Fig. 4.

In Fig. 4, the IR-UWB signal at the input of the central node is the signal *s(t)* from Fig. 2. This signal is used to modulate an optical carrier generated by a laser source, which is accomplished by using a Mach-Zehnder modulator. The resulting optical signal is then transmitted along 80 km of optical fiber until the local exchange. At the local exchange, the EDFA compensates the power losses, as mentioned before, and handles the signal to an optical filter. The optical filter represents the effect of the demultiplexer in Fig. 3 over the isolated channel, contributing as well to reduce the optical noise power incident on the photodetector. After passing through the optical splitter, the signal is transmitted through 0 to 20 km of optical fiber to each one of the customers. In the customers' premises, the optical signal is converted to the electrical domain by a positive-intrinsic-negative (PIN) photodetector and filtered by an electrical filter, which reduces the noise power and the inter-symbol interference (ISI) of the received signal. This signal is then delivered to the receiving antenna subsystem shown in Fig. 2, following which is the IR-UWB receiver.

IV. Performance Evaluation Method

Considering the final application of the system, it is important to assess the effect that the long reach FTTH network has on the original IR-UWB signal. In this context, the performance of the system is evaluated by assessing three parameters: the temporal distortion factor, *TDF*, the spectral distortion factor, *SDF*, and the channel probability of error.

Since the optimum IR-UWB receivers are based on the correlation between the received signal and a known ideal IR-UWB base pulse to estimate the transmitted symbol, it is critical to the system performance that the discrepancies introduced in the received signal by the FTTH network are minimized. In order to assess these discrepancies, the temporal distortion factor is calculated as the correlation between the temporal waveform of the signal radiated by an antenna connected to the electrical filter in Fig. 4, $y_r(t)$, and the original IR-UWB signal radiated by an imaginary antenna connected at the input of the Mach-Zehnder modulator, $s_r(t)$, as depicted in Fig. 5. The temporal distortion factor is given by [13]:

$$TDF = 1 - \frac{\langle s_r(t), y_r(t) \rangle}{\sqrt{\langle s_r(t), s_r(t) \rangle \cdot \langle y_r(t), y_r(t) \rangle}}, \qquad (2)$$

where $\langle \cdot, \cdot \rangle$ represents the inner product between two signals. In the same way, the spectral distortion factor is determined as the correlation between the power spectral density of the signal radiated by the antenna connected to the electrical filter, $S_y(f)$, and the power spectral density of the signal radiated by the imaginary antenna connected to the input of the Mach-Zehnder modulator, $S_s(f)$.

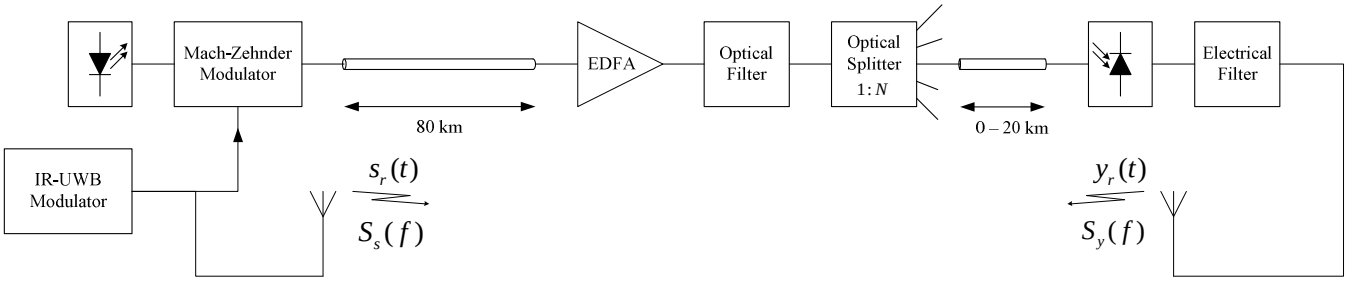

Fig. 5 System model considered for the evaluation of the temporal and spectral distortion factors

The spectral distortion factor is given by:

$$SDF = 1 - \frac{\langle S_s(f), S_y(f) \rangle}{\sqrt{\langle S_s(f), S_s(f) \rangle \cdot \langle S_y(f), S_y(f) \rangle}}. \quad (3)$$

Additionally, the channel error probability is also evaluated. The channel error probability is calculated using a Gaussian approach [14], considering the process of symbol detection after the electrical filter shown in Fig. 5. This approach was considered, in order to isolate the error probability due to the transmission over the FTTH network from the end-to-end error probability (from the IR-UWB modulator until the IR-UWB receiver), which would also include the error probability in the transmission over the air between the antennas. The channel error probability results are presented in the form of *Q* factor, which is related to the error probability, P_e, by:

$$P_e = \frac{1}{2} \cdot \mathrm{erfc}\left(\frac{Q}{\sqrt{2}}\right), \quad (4)$$

where erfc*(x)* is the complementary error function.

Using the three parameters defined above, the system performance was assessed for different values of the bias and modulating voltage of the Mach-Zehnder modulator, respectively, V_b and V_{1max}, for different types and bandwidths of the electrical filter and finally, for the different types of IR-UWB signals defined in Section 2, which complied with the FCC standard.

V. Numerical Results

Two main scenarios have been considered for the evaluation of system performance in this work: one in a back-to-back configuration and another one considering transmission along the optical fiber in the linear regime, for the transmission distances depicted in Fig. 4. The results were obtained considering an optical amplifier (EDFA) with 30 dB gain, a 1:64 optical splitter and a commercially available optical fiber with 0.20 dB/km attenuation coefficient and 18.0 ps/nm/km dispersion coefficient [16].

A. Temporal distortion factor

Fig. 6 depicts the results obtained for the system performance measured in terms of the temporal distortion factor as a function of the Mach-Zehnder modulator parameters. The results are presented as a function of V_{1max}/V_π and for different values of V_b/V_π, where V_π is the modulator's transition voltage (the voltage for which the induced phase difference in each arm of the modulator is π), considering the presence of a 6th order Butterworth electrical filter with 9 GHz bandwidth at the receiver, and the transmission of an IR-UWB signal whose base pulse is the 3rd derivative of the gaussian pulse with α = 150 ps and T_{rep} = 600 ps. In the back-to-back situation, the results show that there is a lower limit for the *TDF*, which was found to be imposed by the presence of the electrical filter in the system. For the situation when there is transmission along the optical fiber, the obtained values are much higher than the ones obtained for the back-to-back situation. Notice that higher values of *TDF* indicate less similarity between the $s_r(t)$ and $y_r(t)$. Acceptable values of *TDF* (meaning a close similarity between those two waveforms) do not exceed 0.1. These results show that, when there is transmission along the optical fiber, the transmitted IR-UWB signal is severely affected by the group velocity dispersion (GVD), which leads to pulse broadening, resulting in a signal that is very different from the original one. It can also be observed in Fig. 6 that, for a constant V_{1max}/V_π value, the best *TDF* values are obtained for V_b/V_π = 1/2 in the back-to-back situation, whereas the best *TDF* values are obtained for V_b/V_π = 5/8 when there is transmission along the optical fiber. This is also due to the effect of GVD.

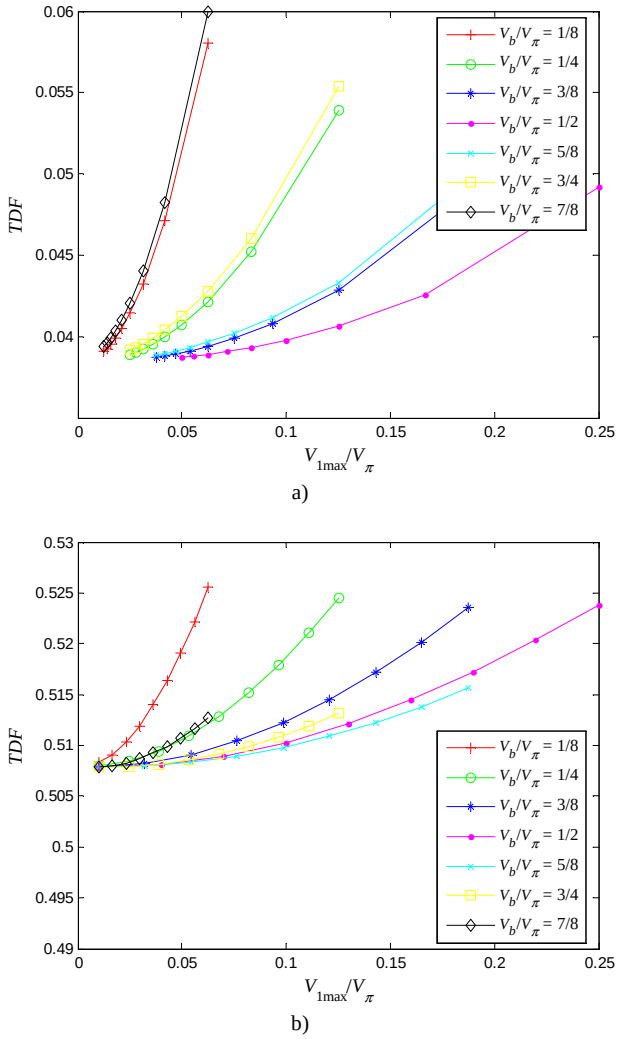

Fig. 6 Temporal distortion factor as a function of V_{1max}/V_π for different V_b/V_π values a) in the back-to-back situation and b) considering the signal transmission along 80 km of optical fiber

In Fig. 7, we present the results obtained for the system

performance measured in terms of the temporal distortion factor as a function of the electrical filter bandwidth, for different types of electrical filters, considering the transmission of an IR-UWB signal whose base pulse is the 3rd derivative of the Gaussian pulse with α = 150 ps and T_{rep} = 600 ps and the the Mach-Zehnder modulator parameters as V_b/V_π = 1/2 and V_{1max}/V_π = 3/16. The obtained results show that, in the back-to-back situation, the *TDF* decreases with increasing bandwidths of the electrical filter, which is the usual behaviour as greater bandwidths of the electrical filter distortion less signal. In case of transmission along the optical fiber, the obtained *TDF* values are much higher than in the back-to-back situation, and seem to have reduced dependence on the electrical filter bandwidth. This is due to the fact that the obtained values are already very high, indicating that a great amount of distortion is introduced due to the propagation along the optical fiber. As a consequence, the presence of the electrical filter will not affect significantly the level of distortion.

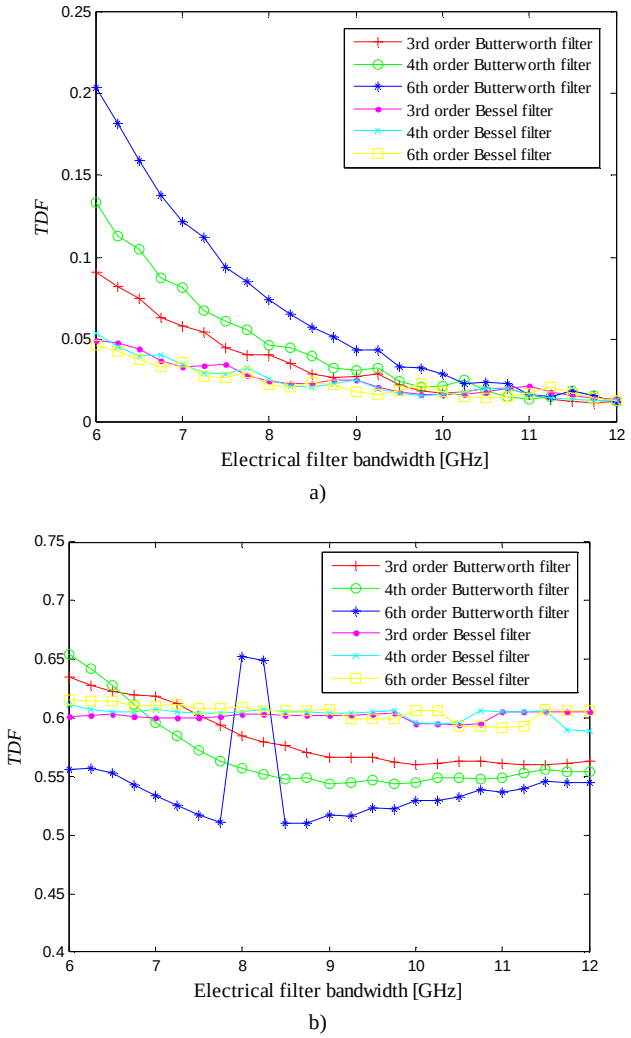

Fig. 7 Temporal distortion factor as a function of the electrical filter bandwidth for different electrical filters a) in the back-to-back configuration and b) considering the signal transmission along 80 km of optical fiber

Regarding the results obtained for *TDF* as a function of the IR-UWB signal characteristics, these are depicted in Fig. 8. The results presented were obtained considering a 6th order Butterworth electrical filter with 9 GHz bandwidth and a Mach-Zehnder modulator with V_b/V_π = 1/2 and V_{1max}/V_π = 3/16, and show that the distortion introduced into the transmitted signal (in both the back-to-back situation and when there is transmission along the optical fiber) is higher for lower shape factor values, and is lower for higher order derivatives of the Gaussian pulse used as base pulse for the IR-UWB signal. The values obtained for the situation when there is transmission along optical fiber are much higher than those obtained in the back-to-back configuration, which explains why there is almost no *TDF* variation with T_{rep} in case of transmission along the optical fiber.

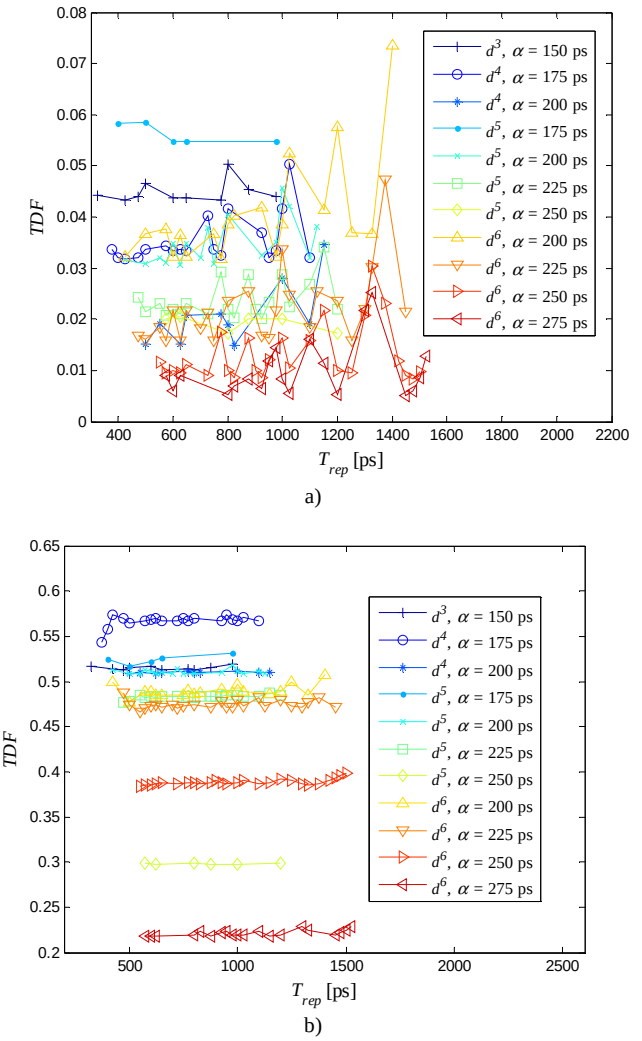

Fig. 8 Temporal distortion factor as a function of the pulse repetition period, T_{rep}, for different shape factors, α, and different derivatives of the gaussian pulse, d^n, used as the base pulse a) in the back-to-back configuration and b) considering the signal transmission along 80 km of optical fiber

B. Spectral distortion factor

In Fig. 9, we present the results obtained for the spectral distortion factor, *SDF*, as a function of the modulator

parameters V_{1max}/V_π for different values of V_b/V_π. These results were obtained under the same conditions of Fig. 6, regarding the electrical filter type and bandwidth, and the transmitted IR-UWB signal. The *SDF* values presented show a similar behaviour to the *TDF* measurements, being considerably higher in case of transmission along the optical fiber. These results indicate that also the spectrum of the signal is severely affected by the GVD. As is known [15], due to the effect of the GVD, the signal spectrum becomes narrower after the transmission along the optical fiber.

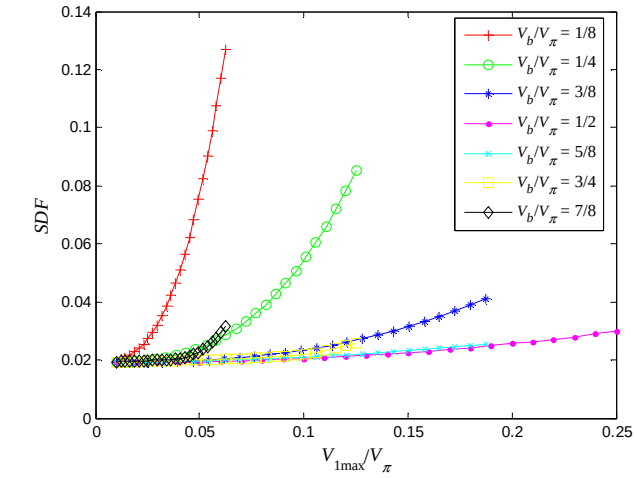

a)

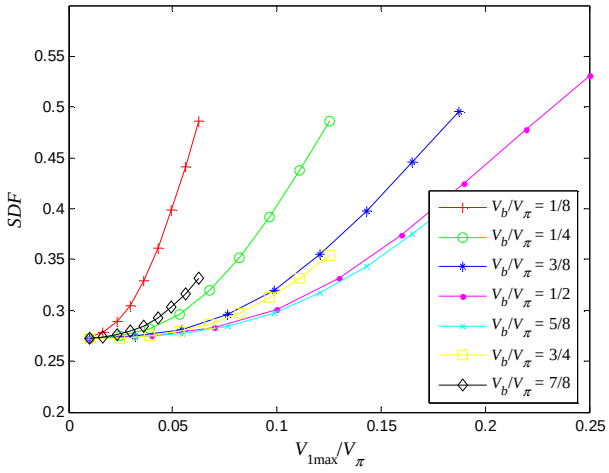

b)

Fig. 9 Spectral distortion factor as a function of V_{1max}/V_π for different V_b/V_π values a) in the back-to-back situation and b) considering the signal transmission along 80 km of optical fiber

In Fig. 10, we present the results obtained for the system performance measured in terms of the spectral distortion factor as a function of the electrical filter bandwidth, for different types of electrical filters, considering the transmission of an IR-UWB signal whose base pulse is the 3rd derivative of the Gaussian pulse with α = 150 ps and T_{rep} = 600 ps and the Mach-Zehnder modulator parameters as V_b/V_π = 1/2 and V_{1max}/V_π = 3/16. The results show that, in the back-to-back situation, the *SDF* is quite low and almost constant for electrical filter bandwidths exceeding approximately 9 GHz. In case of transmission along the optical fiber, there is an optimum electrical filter bandwidth for which *SDF* reaches its lowest value. This optimum point depends on the type of filter and is the result of the distortion caused by the electrical filter itself and the distortion caused by the GVD effect. In fact, for lower electrical filter bandwidths, the distortion is mainly introduced by the electrical filter whereas, for greater electrical filter bandwidths, the distortion is mainly caused by the effect of GVD during the signal propagation along the optical fiber.

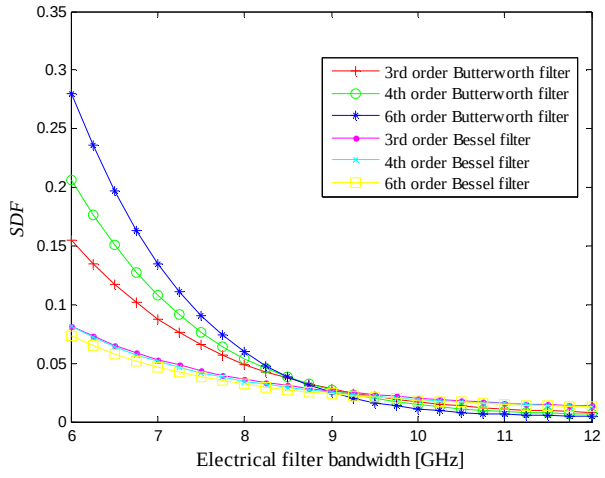

a)

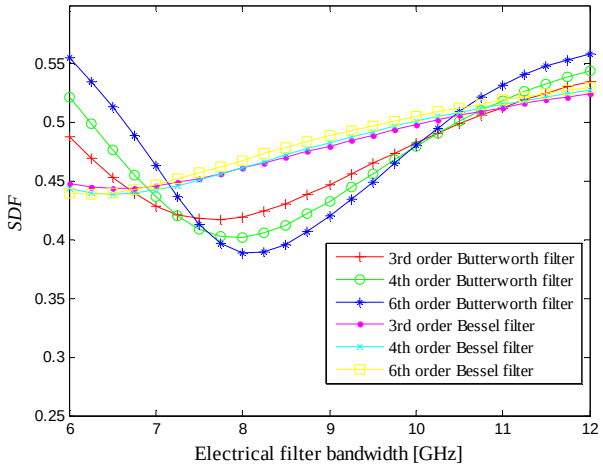

b)

Fig. 10 Spectral distortion factor as a function of the electrical filter bandwidth for different electrical filters a) in the back-to-back configuration and b) considering the signal transmission along 80 km of optical fiber

Fig. 11 depicts the results obtained for the spectral distortion factor as a function of the IR-UWB signal characteristics. The results presented were obtained considering a 6th order Butterworth electrical filter with 9 GHz bandwidth and a Mach-Zehnder modulator with V_b/V_π = 1/2 and V_{1max}/V_π = 3/16. Fig. 11 shows that the distortion introduced in the signal spectrum is significantly higher in case of transmission along the optical fiber compared to the distortion introduced in the back-to-back configuration.

Additionally, with transmission along the optical fiber, the *SDF* increases with increasing shape factor values whereas, in the back-to-back configuration, the *SDF* decreases with increasing shape factor values. In any case, the *SDF* seems independent of the pulse repetition period, T_{rep}, having an almost constant value for each analyzed combination of the shape factor value and the order of the Gaussian pulse derivative used as base pulse for the IR-UWB signal.

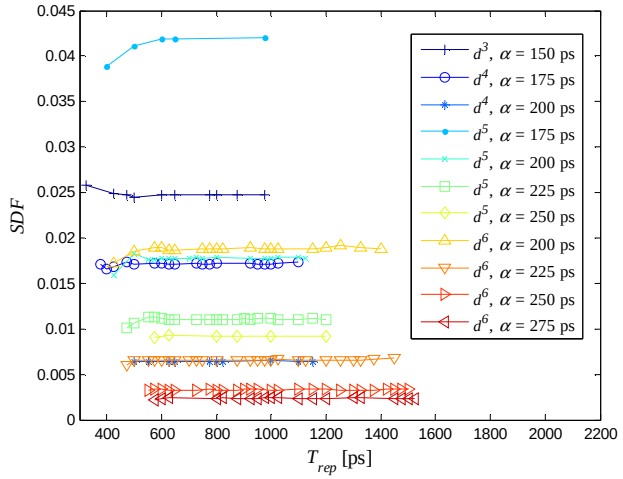

a)

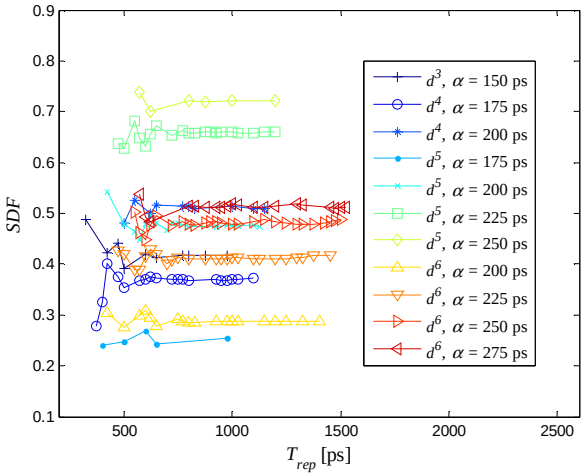

b)

Fig. 11 Spectral distortion factor as a function of the pulse repetition period, T_{rep}, for different shape factors, α, and different derivatives of the gaussian pulse, d^n, used as the base pulse a) in the back-to-back configuration and b) considering the signal transmission along 80 km of optical fiber

voltage for V_b/V_π = 1/2. Also in the case of transmission along the optical fiber, the best performance is achieved for the situation where V_b/V_π = 1/2. However, a significant degradation of the *Q* factor is observed in this case, which is the result of the GVD occurring during the signal propagation along the optical fiber. Some of the values obtained for the *Q* factor, in the case of transmission along the optical fiber, are still quite acceptable ($Q \geq 7$, which corresponds to $P_e \leq 10^{-12}$).

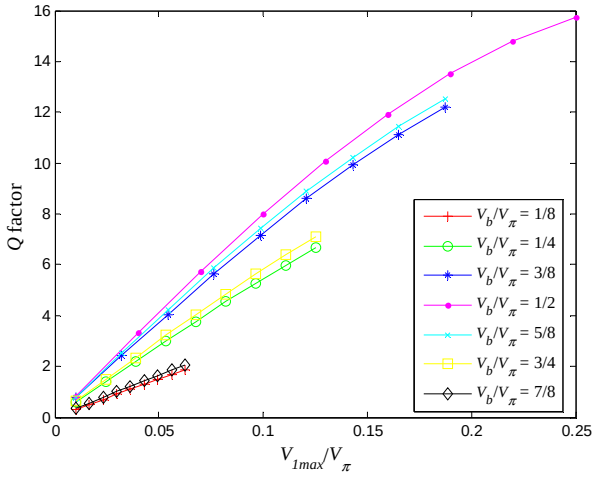

a)

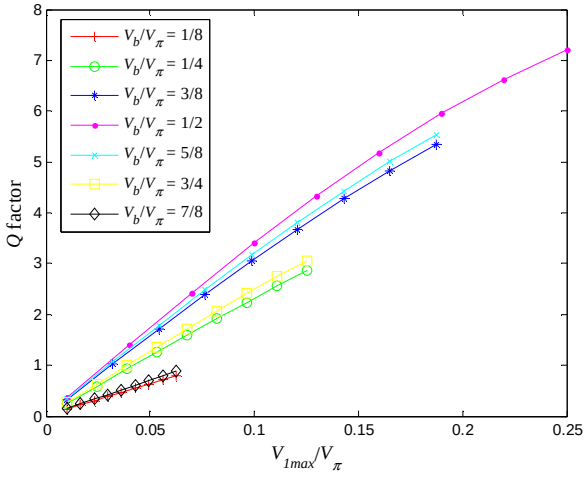

b)

Fig. 12 *Q* factor as a function of V_{1max}/V_π for different V_b/V_π values a) in the back-to-back situation and b) considering the signal transmission along 80 km of optical fiber

C. *Channel error probability*

Regarding the system performance measured in terms of the channel probability of error, the results are shown in Fig. 12 for the *Q* factor as a function of V_{1max}/V_π for different values of V_b/V_π. The obtained results for the back-to-back configuration show that, for the same V_{1max}/V_π value, the best performance (higher value of the *Q* factor) is achieved when V_b/V_π = 1/2. This is due to the fact that the Mach-Zehnder modulator characteristic is the most linear with respect to its modulating

Fig. 13 shows the results obtained for the system performance measured in terms of the channel error probability as a function of the electrical filter bandwidth, for different types of electrical filters. We consider the transmission of an IR-UWB signal whose base pulse is the 3rd derivative of the Gaussian pulse with α = 150 ps and T_{rep} = 600 ps and the the Mach-Zehnder modulator parameters as V_b/V_π = 1/2 and V_{1max}/V_π = 3/16. The results obtained for the back-to-back situation show that the optimum filter bandwidth (which corresponds to the simultaneous minimization of the signal amplitude distortion caused by the filter and of the noise

introduced by the optical amplifier and electrical receiver) increases with increasing orders of the Butterworth electrical filter and is identical for any order of the Bessel filters, which is due to the amplitude response of each of these filters.

In case of transmission along the optical fiber, the results show a degradation on the performance of the system for increasing bandwidths of the electrical filter. By increasing the bandwidth of the electrical filter, higher optical and electrical noise powers are present at the filter output, degrading the overall optical signal-to-noise ratio (OSNR) and electrical signal-to-noise ratio, and consequently increasing the channel error probability.

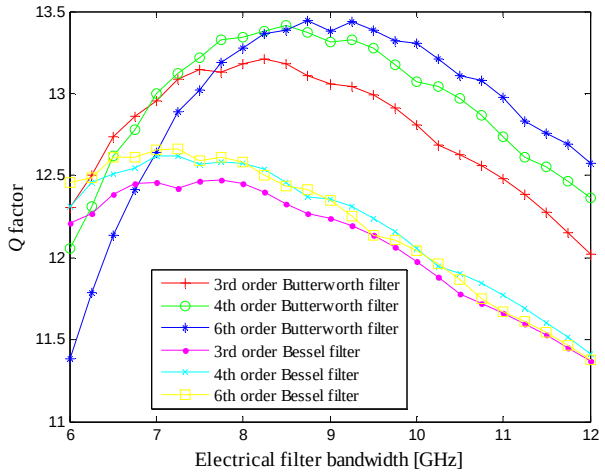

a)

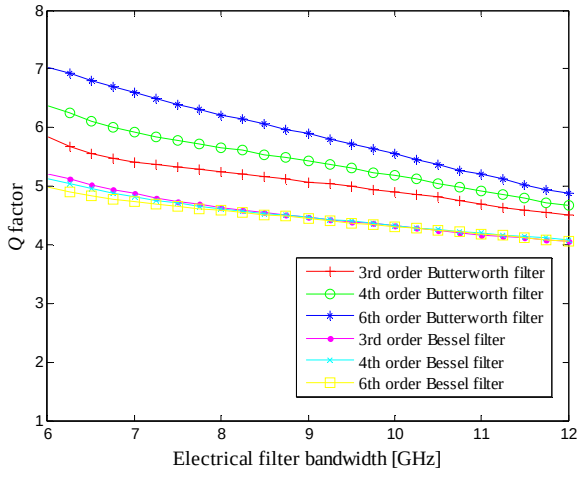

b)

Fig. 13 *Q* factor as a function of the electrical filter bandwidth for different electrical filters a) in the back-to-back configuration and b) considering the signal transmission along 80 km of optical fiber

Regarding the system performance measured in terms of the channel error probability, the results are shown in Fig. 14 as a function of the IR-UWB signal characteristics. The results presented were obtained considering a 6th order Butterworth electrical filter with 9 GHz bandwidth and a Mach-Zehnder modulator with V_b/V_π = 1/2 and V_{1max}/V_π = 3/16, and show that in the back-to-back configuration and the situation when there is transmission along the optical fiber, the channel probability of error decreases (*Q* factor increases) with increasing values of the shape factor, α. Additionally, it is also perceptible, for both the situations presented, that changes in the pulse repetition period, T_{rep}, do not have a significant effect on the values obtained for the channel error probability. This is due to the fact that the *duty-cycle* of the IR-UWB signals is very low, and therefore, the induced inter-symbol interference caused by the GVD effect during the propagation along the optical fiber, is reduced.

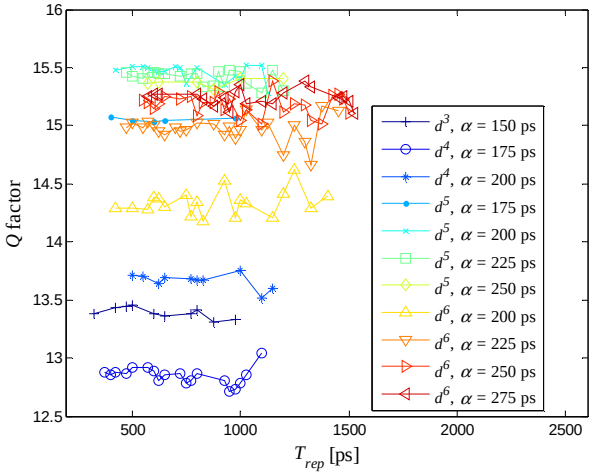

a)

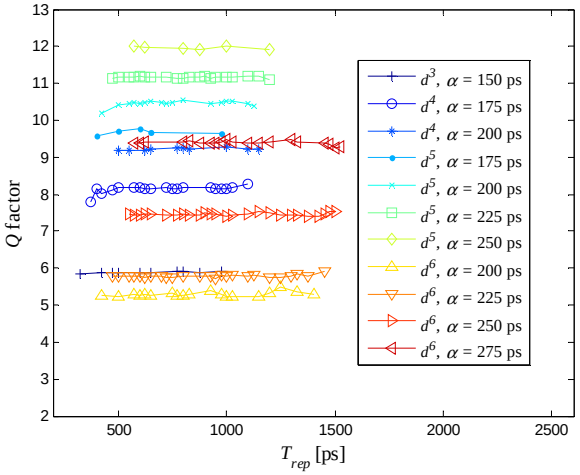

b)

Fig. 14 *Q* factor as a function of the pulse repetition period, T_{rep}, for different shape factors, α, and different derivatives of the gaussian pulse, d^n, used as the base pulse a) in the back-to-back configuration and b) considering the signal transmission along 80 km of optical fiber

VI. Conclusions

The results obtained show that the performance of the system, measured in terms of the temporal and spectral distortion factors, is severely degraded with the transmission distance. This is mainly due to the effect of time-broadening of the transmitted pulses caused by the group velocity dispersion, which occurs during the signal propagation along the optical

fiber. Although the spectrum of the signal is also changed due to this effect, it has been verified that, in most cases, the signal after transmission through the system is still able to comply with the FCC requirements. Additionally, it has been confirmed that the degradation occurred in the channel error probability is quite low allowing for the correct detection of the transmitted symbols after the electrical filter. The results presented suggest that the effect of GVD is the major impairment for the implementation of the distribution of IR-UWB signals with PAM modulation in FTTH networks since the signal distortion due to that effect affects severely the waveform, preventing the correct signal detection by means of a correlation receiver, as used in common IR-UWB networks.

VII. References

[1] Title 47, Section 15 of the Code of Federal Regulations SubPart F: "*Ultra-wideband, Federal Communications Commission*"

[2] Siriwongpairat, W. P. and Ray Liu, K. J., "*Ultra-Wideband Communication Systems: Multiband OFDM Approach*", John Wiley & Sons, Inc.

[3] Di Benedetto, M., Kaiser, T., Molisch, A.F., Oppermann, I., Politano, C. and Porcino, D., "*UWB Communication Systems – A Comprehensive Overview*", Hindawi Publishing Corporation, 2006

[4] Di Benedetto, M. and Giancola, G., "*Understanding Ultra Wide Band Radio Fundamentals*", Prentice Hall PTR, 2004

[5] Llorente, R., Alves, T., Morant, M., Beltran, M., Perez, J., Cartaxo, A. and Marti, J., "*Optical distribution of OFDM and Impulse-Radio UWB in FTTH networks*", Conference on Optical Fiber communication, Feb. 2008, pp. 1-3

[6] Llorente, R., Alves, T., Morant, M., Beltran, M., Perez, J., Cartaxo, A. and Marti, J. "*Ultra Wide-Band radio signals distribution in FTTH networks*", IEEE Photonics Technology Letters, Vol. 20, No. 11, pp. 945 - 947, June, 2008

[7] Dai, Y. and Yao, J., "*An approach to optical generation and distribution of binary phase coded direct sequence ultra-wideband signals*", 2007 IEEE International Topical Meeting on Microwave Photonics, pp. 257-260

[8] Talli, G. and Townsend, P. D., "*Hybrid DWDM-TDM long-reach PON for next-generation optical access*", Journal of Lightwave Technology, Vol. 24, No. 7, pp. 2827-2834, July 2006

[9] Sheng, H., Orlik, P., Haimovich, A. M., Cimini, L. J. and Zhang, J., "*On the Spectral and Power Requirements for Ultra-Wideband Transmission*", Mitsubushi Electric Research Laboratories, TR2003-66, December 2003

[10] Townsend, P. D., Talli, G., Chow, C. W., MacHale, E. M., Anthony, C., Davey, R., De Ridder, T., Qiu, X. Z., Ossieur, P., Krimmel, H. G., Smith, D. W., Lealman, I., Poustie, A., Randel, S. and Rohde, H. "*Long Reach Passive Optical Networks*", The 20th Annual Meeting of the IEEE Laser and Electro-Optics Society, 2007 (LEOS 2007), pp. 868-869

[11] Photonic Integrated Extended Metro and Access Network, http://www.ist-pieman.org

[12] Davey, R.P., Healey, P., Hope, I., Watkinson, P. and Payne, D.B., "*DWDM reach extension of a GPON to 135 km*", Journal of Lightwave Technology, Vol. 24, Issue 1, pp. 29-31, Jan. 2006

[13] Jazayerifar, M., Cabon, B. and Salehi, J., "*Transmission of multi-band and impulse radio Ultra-Wideband signals over single mode fiber*", Journal of Lightwave Technology, Vol. 26, No. 5, Aug. 2008, pp. 2594-2603

[14] Rebola, J. L. and Cartaxo, A. V. T, "*Gaussian approach for performance evaluation of optically preamplified receivers with arbitrary optical and electrical filters*", IEE Proceedings – Optoelectronics, Vol. 148, No. 3, Junho 2001

[15] Agrawal, G. P., "Nonlinear Fiber Optics", Academic Press, 2001

[16] "*Corning® SMF-28e® XB Optical Fiber – Product Information*", Corning Incorporated, Oct. 2008